Towards numerical modelling of THMC coupled processes in fractured geothermal reservoirs

Saeed Salimzadeh[1], Hamidreza M. Nick[2], Adriana Paluszny[1], David F. Bruhn[3]

[1] Imperial College London

[2] Technical University of Denmark

[3] Delft University of Technology

hamid@dtu.dk

Keywords: Hydraulic fracturing, thermal non-equilibrium, thermoelasticity, enhanced geothermal systems.

ABSTRACT

Sustainable and successful energy recovery from deep geothermal reservoirs requires a comprehensive understanding of how different local scale physical and chemical processes affect the short and long term heat transport. Geothermal aquifers may be utilized for storing CO2 through dissolution of CO2 in the return (cold) water stream of geothermal doublets. The safety and performance of operations highly depends on reservoir physical, thermal, and compositional properties, which may change following cooled water injection and potential reactions. Yet, the emergent behaviour of the system due to the interaction of thermal, flow, mechanical and chemical processes is not fully understood. We present a new framework permitting coupled simulation of Thermal-Hydro-Mechanical (THM) processes in geothermal reservoirs. The approach simultaneously couples non-isothermal laminar flow through fractures and Darcy flow through the rock matrix with thermoporoelastic deformation. This framework easily lend itself for modelling reactive transport in fractured geothermal reservoirs. The coupled THM model is validated against several benchmark examples and employed to study the effect of THM processes on energy production in a geothermal doublet.

1. INTRODUCTION

Geothermal power production has become an attractive energy resource. Transport properties of saturated porous media is affected by thermal-hydro-mechanical (THM) effects as well as by chemical reactions (Blocher et al, 2010; Izadi and Elsworth, 2015). In fractured geothermal reservoirs, fluid is often not in thermal equilibrium with the surrounding solid rock, leading to a heat transfer phenomenon taking place between the fluid inside the fracture and the host solid through the fractures surfaces. Heat transfer between the fluid inside fracture and surrounding rock solid has been of particular interest in many cases including magma-driven fractures (Spence and Turcotte, 1985), hydraulic fracturing wells (Wang and Papamichos, 1999), hydraulic fracturing of gas shale (Tran et al., 2013; Enayatpour and Patzek, 2013; Abousleiman et al., 2014), stability of geothermal wells (Hals and Berre, 2013; Pogacnik et al., 2016), crack propagation in fuel cells (Shao et al., 2015), and geothermal reservoirs (Ghasemi et al., 2008; Izadi and Elsworth, 2015). In the analytical contributions, it is common to assume constant rock temperature at the surfaces of the hydraulic fracture/well, equal to the temperature of the injected fluid (Wang and Papamichos, 1999; Tran et al., 2013; Abousleiman et al., 2014). Such an assumption does not satisfy conservation of energy, and does not account for the fact that heat exchange between the fracturing fluid and the rock gradually causes the fracturing fluid to thermally equilibrate with the matrix rock. Consequently, an unrealistically large effect due to thermal non-equilibrium is predicted by such approaches, for instance, complete fracture closure in the case of hot water injection (Tran et al., 2013).

In the present study, a robust finite element model for flow through discrete fractures in permeable rocks is presented. Local thermal non-equilibrium is considered between fracture fluid, matrix fluid and solid rock. The model simultaneously accounts for non-isothermal laminar flow in discrete fractures, non-isothermal Darcy flow in the rock matrix, and heat conduction in the rocks. Heat exchanges between fracture fluid, matrix fluid and solid medium are defined based on the temperature gradients. The model also accounts for fracture growth using Linear Elastic Fracture Mechanics (LEFM) concept by computing modal stress intensity factors for two-dimensional fractures in three-dimensional models. The direction of growth is estimated using energy-based criteria which observe the relationship between modal stress intensity factors and how it varies along the tip (Paluszny and Zimmerman, 2013). The model is validated against available several benchmark examples. A geothermal doublet is modelled and the initial results are presented.

2. COMPUTATIONAL MODEL

The fully coupled computational model is constructed from six interacting sub-models: a thermoporoelastic mechanical model, two flow models for fractures and rock matrix, and three heat transfer models for the rock solid, the matrix fluid, and the fracture fluid. The thermoporoelastic mechanical model, the matrix flow model, the matrix convective (conduction and advection) heat transfer model, and the solid conductive heat transfer model are constructed for three-dimensional body, while the flow and the convective heat transfer through the fractures are defined for two-dimensional discrete fractures.

2.1 Poroelastic Models

The thermoporoelastic mechanical model is based on the condition of stress equilibrium for a representative elementary volume of the porous medium. Effective stress is defined as the function of total stress and matrix pressure that controls the mechanical effects of a change in stress. It is defined exclusively within the rock matrix, linking a change in stress to the change in strain. The stress-strain relationship for thermoelasticity can be written as (Khalili and Selvadurai, 2003)

$$\boldsymbol{\sigma}' = \mathbb{D}\boldsymbol{\varepsilon} - \beta_s K T_s \mathbf{I} \qquad [1]$$

in which σ^' is the effective stress, D is the drained stiffness matrix, ε is the strain, β_s is known as the coefficient of volumetric thermal expansion of the rock, K is bulk modulus of rock, T_s is the solid (rock) temperature, and I is the second-order identity tensor. Assuming negligible shear tractions exerted from the fluid on the fracture walls, which is consistent with the lubrication approximation (Spence and Turcotte, 1985), the normal tractions on the fracture surface can be written as

$$\mathbf{T}_c = -p_f \mathbf{n}_c \qquad [2]$$

where p_f is the fluid pressure in the fracture i.e. fracture pressure, and $\mathbf{n}_c$ is the outward unit normal to the fracture surface. The thermoporoelastic governing equation for the deformation field of a porous rock can be rewritten as

$$\mathrm{div}\left(\frac{1}{2}\mathbb{D}(\nabla\mathbf{u} + \mathbf{u}\nabla) - \alpha p_m \mathbf{I} - \beta_s K T_s \mathbf{I}\right) - p_f \mathbf{n}_c + \mathbf{F} = 0 \qquad [3]$$

where, **u** is the solid displacement vector, α is the Biot coefficient, p_m is the fluid pressure in the matrix, i.e. matrix pressure, and F is the body force.

The matrix flow model that represents the flow through the porous matrix (porous rock) is constructed by combining Darcy's law with mass conservation for the fluid. An independent fracture flow model is considered for fracture discontinuities. This allows direct computation of fracture pressures and explicit application of hydraulic pressures on sub-dimensional fracture walls. The objective is to obtain a more realistic representation of fracture flow. Assuming a high aspect ratio fracture that has a surface much larger than its aperture; the average velocity of a fluid along the fracture surface can be approximated using the cubic law as (Witherspoon et al. 1980)

$$\mathbf{v}_f = -\frac{{a_f}^2}{12\mu_f}\nabla p_f \qquad [4]$$

where a_f is the fracture aperture, defined as the differential displacement between two walls of the fracture, $a_f = (\mathbf{u}^+ - \mathbf{u}^-).\mathbf{n}_c$, μ_f is the fracture fluid dynamic viscosity, and p_f is the fracture fluid pressure. $\mathbf{u}^+$ and $\mathbf{u}^-$ represent displacements on two opposite sides of the fracture. Pressurised fluid can leak from the fracture into the permeable rock matrix and vice versa, known as leak-off. Assuming linear pressure gradient between the fracture and the connected matrix, the leak-off flow per unit area of the fracture wall can be written as

$$\mathcal{L}_f = \rho_f c_L (p_m - p_f) \qquad [5]$$

where, p_m and p_f are the matrix and fracture fluid pressures, respectively, $c_L = \frac{k_m}{\mu_f y}$ is the leak-off coefficient, in which, k_m is the matrix permeability, μ_f is the fluid viscosity, and y is the distance between the fracture and the centre of the connected matrix (volume) element (Salimzadeh and Khalili, 2015a). The governing equation for laminar flow through the fracture in non-isothermal conditions can be written as

$$\mathrm{div}\left(\frac{{a_f}^3}{12\mu_f}\nabla p_f\right) = \frac{\partial a_f}{\partial t} + a_f c_f \frac{\partial p_f}{\partial t} - a_f \beta_f \frac{dT_f}{dt} - c_L(p_p - p_f) \qquad [6]$$

where T_f is the temperature of the fluid inside the fracture. Note that the term $\frac{\partial a_f}{\partial t} = \frac{\partial (\mathbf{u}^+ - \mathbf{u}^-).\mathbf{n}_c}{\partial t}$ provides explicit coupling between the displacement field and the fracture flow field (Salimzadeh and Khalili, 2015b). The governing equation for laminar flow through the fracture in non-isothermal conditions reduces to the lubrication equation (Batchelor, 1967) for the case of one-dimensional incompressible flow in impermeable matrix under isothermal conditions, i.e. $c_f = 0, c_L = 0, \frac{dT_f}{dt} = 0$, as

$$\frac{1}{12\mu}\frac{\partial}{\partial s}\left({a_f}^3 \frac{\partial p_f}{\partial s}\right) = \frac{\partial a_f}{\partial t} \qquad [7]$$

where s is the distance along the fracture length.

2.2 Heat Transfer Models

The governing equation for heat transfer through the solid rock can be achieved by combining Fourier's law with the energy balance equation for solids (Tong

et al., 2010; Gelet et al., 2012). The balance of energy accounts for the flux of thermal energy due to conduction, the rate of entropy for solid, and the rate of energy exchange between solid and fluid. The heat transfer between solid and the fluid in the matrix and in the fracture can be written respectively as

$$q_{sm} = c_{Tm}(T_s - T_m) \quad [8]$$

$$q_{sf} = c_{Tf}(T_s - T_f) \quad [9]$$

where, c_{Tm} and c_{Tf} are the solid-fluid heat exchange coefficients for matrix and fracture, respectively. T_f and T_f are the matrix and fracture fluid temperatures, i.e. matrix temperature and fracture temperature, respectively. The solid-fluid heat exchange coefficients can be estimated from solid thermal conductivity.

The governing equations for heat transfer through fluid in the fracture and in the rock matrix can also be achieved by combining Fourier's law with energy balance for fluid. However, the balance of energy additionally accounts for the advective heat transfer in the moving fluid. Therefore, the convective heat transfer (conduction + advection) in the matrix fluid can be written as

$$\mathbf{q}_f = -\boldsymbol{\lambda}_f \nabla T_f + \rho_f C_f T_f \mathbf{v}_f \quad [10]$$

where $\mathbf{q}_f$ is the convective heat flux through the fluid, $\boldsymbol{\lambda}_f$ is the thermal conductivity tensor of the fluid, ρ_f is the fluid density, C_f is the fluid specific heat capacity, and $\mathbf{v}_f$ is the fluid velocity. Heat is also exchanged between matrix and fracture fluids through leak-off mass exchange term

$$\mathbf{q}_{mf} = \mathcal{L}_f C_f (T_m - T_f) \quad [11]$$

where $\mathcal{L}_f$ is the leak-off fluid.

2.3 Finite Element Approximation

Governing equations are solved numerically using the finite element method. Galerkin method and finite difference techniques are used for spatial and temporal discretisation, respectively. Displacement vector **u**, fluid pressures p_m and p_f, and solid and fluid temperatures T_s, T_m and T_f are defined as the primary variables. Using the standard Galerkin method, the primary variable $\mathbf{X} = \{\mathbf{u}, p_m, p_f, T_s, T_m, T_f\}$ within an element is approximated from its nodal values as

$$\mathbf{X} = \mathbf{N}\hat{\mathbf{X}} \quad [18]$$

where **N** is the vector of shape functions and $\hat{\mathbf{X}}$ is the vector of nodal values. Using the finite difference technique, the time derivative of **X** is defined as

$$\frac{\partial \mathbf{X}}{\partial t} = \frac{\mathbf{X}^{t+dt} - \mathbf{X}^t}{dt} \quad [19]$$

where $\mathbf{X}^{t+dt}$ and $\mathbf{X}^t$ are the values of **X** at time $t+dt$ and t, respectively. The set of discretised equations can be written in matrix form of **SX=F**, in which **S** is the element's general stiffness matrix, and **F** is the vector of right-hand-side loadings.

2.4 Fracture Growth Computation

The mechanical deformation of rocks leads to concentrations of stress around fracture tips, which can be quantified locally at each tip by the stress intensity factors (SIFs). The SIFs are key parameters in evaluating and predicting fracture growth and the potential growth direction, and take into account the effects of mechanics and fluids on the growth of the fracture. The state of stress immediately ahead of the fracture front is known to be singular. Two methods for the SIF extraction from the FE solution can be employed. Direct approaches, based on the correlation of the displacements over the crack surface are simple, straightforward, and computationally inexpensive; require very refined meshed around the crack front in order to yield low approximation error. Alternatively, energy based methods which integrate the region ahead of the crack tip are less prone to numerical error and yield better approximations with significantly coarser meshes. Three stress intensity factors for three modes of fracture opening are computed by computing the energy-based I-Integral (Yau et al., 1980) over a set of virtual disk domains distributed along the fracture tip (Nejati et al., 2015). The three SIFs are mode I for opening due to tensile loading, mode II for in-plane shearing due to sliding, and mode III for out-of-plane shearing due to tearing. These are computed locally at 100 locations along the fracture front, and are used to determine if the fracture will or will not advance. Fractures are extended by deforming their geometry, details of this method can be found in Paluszny & Zimmerman (2011).

3. SIMULATION RESULTS

3.1 Hydraulic Fracturing Example

Fluid is injected into centre of a radial (penny-shaped) fracture of initial radius 1 m. Hydraulic fractures grow in a plane perpendicular to the direction of minimum in situ stress. Minimum in situ stress is set to 10 MPa. The rock's mechanical properties: Young's modulus, Poisson's ratio, and fracture toughness are set to 17 GPa, 0.2, and 1 MPa $m^{0.5}$, respectively. A block of size 90×90×60 m is modelled with a radial fracture of initial radius of 1 m in its centre. The fracturing fluid has a viscosity of 0.1 Pa s, and is injected at a rate of 0.001 m^3/s. The fracture is growing when mode I stress intensity factor exceeds the fracture toughness. Three cases are simulated: in case 1 the permeability of the rock matrix is set to zero, while in the other two cases, the permeability is set to 10^{-13} m^2. In case 2, the permeability of the rock is assumed only in the direction perpendicular to the fracture surface (1D leak-off), while in case 3 the permeability is assumed homogeneous (3D leak-off).

The results for the hydraulic fracturing variables: injection pressure, fracture aperture and fracture length are shown in Figures 1-3, respectively.

Included in these figures are the analytical solutions by Savitski and Detournay (2002) for the viscosity-storage regime. Very good agreement found between simulated results for case 1 (zero leak-off) with the analytical solutions confirming the accuracy of the hydromechanical model. When the leak-off is allowed, the injection pressure increases, while the fracture aperture and the fracture length reduce. The more leak-off, the more increase in injection pressure and reduction in fracture aperture and length. Therefore, when the leak-off is three-dimensional (3D), it further increases injection pressure and reduces fracture aperture and length. Included in Figure 3 is the analytical solution for leak-off dominated case (Garagash et al., 2011). The simulation results lie between the two extremes (storage and leak-off) meaning that the simulated cases do not belong to any of those extremes. This highlights the importance of a robust numerical model where there is no analytical solution available.

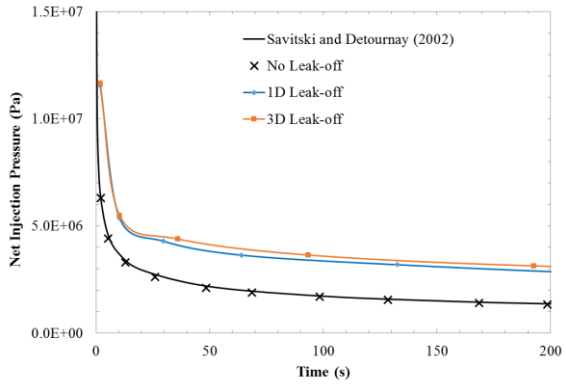

Figure 1: Net injection pressure versus injection time in hydrofracking example.

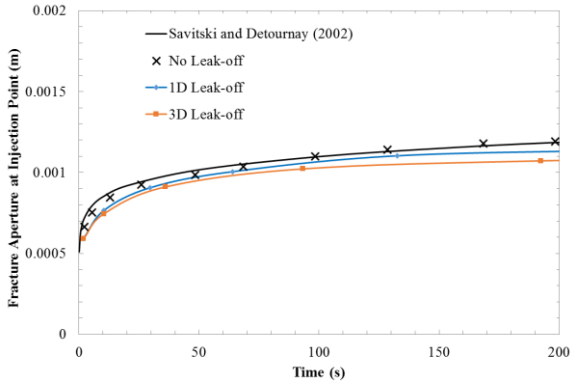

Figure 2: Fracture aperture at the injection versus injection time in hydrofracking example.

3.2 Advective-Diffusive Heat Transfer through a Single Fracture

In this example, a fracture of length 100 m and width 50 m is considered between injection and production wells. Water is injected at relative temperature of -100 ℃, while rock's initial temperature is set to zero. The matrix is considered to be impermeable. The water and solid properties are given in Table 1.

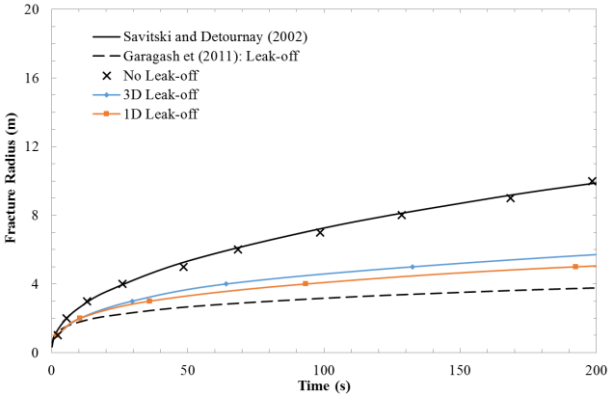

Figure 3: Fracture radius versus injection time in hydrofracking example.

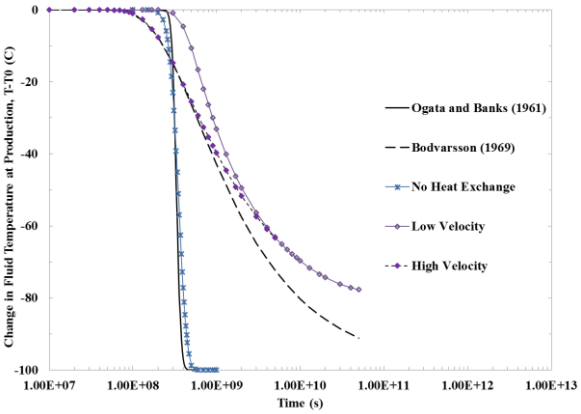

Figure 4: Change in fluid temperature at production versus time in advective-diffusive heat transfer example.

Three cases are considered: in case 1 the heat exchange between fluid in the fracture and solid is neglected, while in the second and third cases, the heat exchange is allowed. Injection rate in case 1 is set to 1.5×10^{-8} m^3/s and in cases 2 and 3 to 1.5×10^{-4} m^3/s. The fluid in the fracture has a constant velocity of 3.0×10^{-7} m/s (low velocity) in cases 1 and 2, and a constant velocity of 3.0×10^{-5} m/s (high velocity) in case 3. The constant velocities are achieved by adjusting constant fracture aperture, accordingly. The results for the fluid's temperature change at the production are shown in Figure 4. Included in this figure are the analytical solution by Ogata and Banks (1961) for advective-diffusive heat transfer through fracture only, as well as solution by Bodvarsson (1969) for heat transfer through fracture and rock. Good agreement found between current results in case 1 with analytical solutions. The temperature of the fluid at the production rapidly decreases as the injected fluid reaches the production well. When the heat exchange between solid and fluid is allowed, heat is transferred to the fluid from the solid leading to gradual change in the fluid temperature at production. Fluid velocity affects the early response of the fluid

temperature while the ultimate response is controlled by the injection rate. That is why the fluid temperature in both cases 2 and 3 converges towards a unique response. Also good agreement found between present results and the analytical solution by Bodvarsson (1969), however, the two results are diverging at the later time. This is due to the fact that the conduction in the solid in the present simulations is considered 2D, while in the analytical solution it is assumed to be 1D and in the direction perpendicular to the fracture.

3.3 A Geothermal Doublet

In this section a geothermal doublet is modelled in which fluid is injected with a relative temperature -100 ℃ (colder than the in situ temperature) through a horizontal well into a radial fracture (in vertical plane) of radius 4m, at a rate of 0.001 m3/s. Production is performed through a vertical well 10m away from the fracture. Four cases are simulated: in case 1 the permeability of the medium is assumed 1D in direction perpendicular to the fracture (and towards the production well), while in case 2 the permeability of the medium is assumed homogeneous in three dimensions. Cases 3 and 4 are duplicates of cases 1 and 2, respectively, however, in these cases the heat transfers in the rock solid and matrix fluid are considered uncoupled, i.e. $c_{Tm} = 0$.

Table 1: Water and rock hydro-thermal properties.

Property Name	Value	Unit
Water Density	1000	Kg/m^3
Water Heat Capacity	4000	J/Kg℃
Water Thermal Conductivity	0.6	W/m℃
Water Thermal Diffusivity	1.5×10^{-7}	m^2/s
Water Volumetric Thermal Expansion	2.07×10^{-4}	1/℃
Water Compressibility	1×10^{-9}	Pa^{-1}
Water Viscosity	0.001	Pa s
Rock Density	2500	Kg/m^3
Rock Heat Capacity	850	J/Kg℃
Rock Thermal Conductivity	2.125	W/m℃
Rock Thermal Diffusivity	1×10^{-6}	m^2/s

The matrix fluid temperature distribution 50 days after the start of injection of cold water for two cases 1 and 2 are shown in Figure 5. Three-dimensional leak-off in case 2 leads to slower fluid movement towards production well, while in one-dimensional case the cold fluid reaches relatively fast to the production well. The temperature changes in the rock and fluid at the production well versus time are shown in Figure 6. When the solid-matrix fluid heat exchange is ignored (cases 3 and 4), the cold matrix fluid travels relatively fast towards production without reaching thermal-equilibrium with the solid. On the other hand, the solid-matrix heat exchanged term couples the heat transfer in the solid with that in the matrix fluid, leading to thermal equilibrium between solid and matrix fluid. Therefore, it takes extended period of time for the cold fluid to reach the production well. Chemical reactions may alter the permeability tensor of the rock, consequently affect the direction of leak-off.

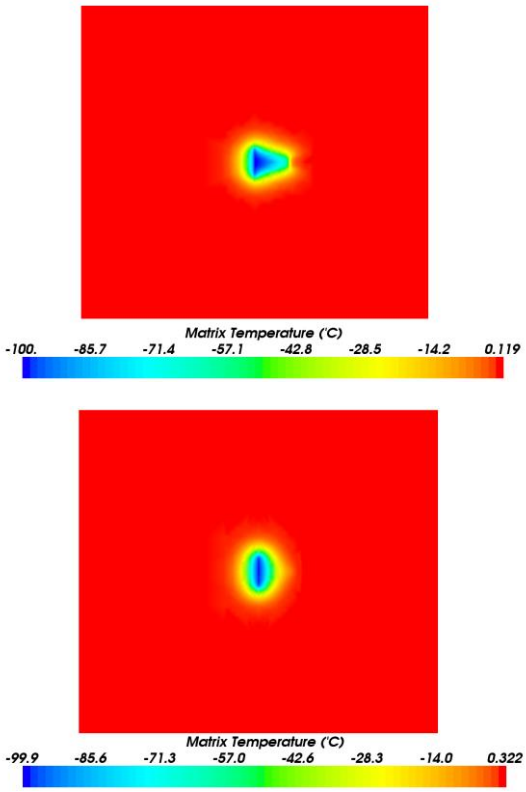

Figure 5: Matrix fluid temperature distribution after 5 days of injection in geothermal doublet. Top: case 1 with one-dimensional leak-off. Bottom: case 2 with three-dimensional leak-off.

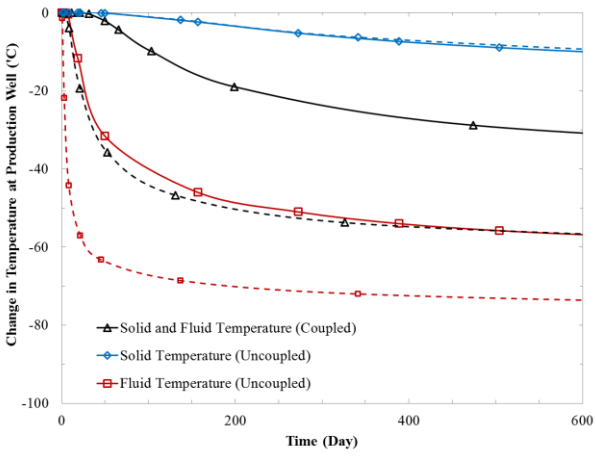

Figure 6: Change in the rock and matrix fluid temperatures at production well versus time in geothermal doublet. One-dimensional leak-off cases (cases 1 and 3) are shown in dashed line while solid lines represent three-dimensional leak-off.

4. CONCLUSIONS

A robust, fully coupled model is presented for simulating non-isothermal flow through deformable fracturing media. The model simultaneously accounts for flow and heat transfer through the fracture and the rock matrix, heat transfer through the rock solid, the rock deformation and fracture propagation. The proposed model has been validated against several benchmark examples and applied to a geothermal doublet. Results show that when the leak-off from the fracture is considered three-dimensional, the injected fluid travels longer distances and covers larger areas, than the case of one-dimensional leak-off. Therefore, it takes longer for the produced fluid to lose its temperature. The effects of chemical reactions might alter the permeability tensor and affect the fluid residence time.

REFERENCES

Abousleiman, Y.N., Hoang, S.K., Liu, C., 2014, Anisotropic porothermoelastic solution and hydro-thermal effects on fracture width in hydraulic fracturing, *Int. J. Numer. Anal. Meth. Geomech*. 2014; 38:493–517.

Blocher, M.G., Zimmermann, G., Moeck, I., Brandt, W., Hassanzadegan, A., Magri, F., 2010, 3D numerical modelling of hydrothermal processes during the lifetime of a deep geothermal reservoir, *Geofluids* 10, 406-421.

Bodvarsson, G., 1969. On the Temperature of Water Flowing through Fractures, *Journal of Geophysical Research*, 74(8), 1987-1992.

Enayatpour, S., Patzek, T., 2013. Thermal Shock in Reservoir Rock Enhances the Hydraulic Fracturing of Gas Shales, *Unconventional Resources Technology Conference held in Denver, Colorado, USA*, 12-14 August 2013.

Garagash, D., Detournay, E., Adachi, J., 2011. Multiscale tip asymptotics in hydraulic fracture with leak-off, *Journal of Fluid Mechanics*, 669, 260-297.

Gelet, R., Loret, B., Khalili, N., 2012. A thermo-hydro-mechanical coupled model in local thermal non-equilibrium for fractured HDR reservoir with double porosity, *Journal of Geophysical Research*, 117, B07205, doi: 10.1029/2012 JB009161.

Ghasemi, A., Nygren, A., Cheng, A., 2008, Effects of heat extraction on fracture aperture: A poro–thermoelastic analysis, *Geothermics* 37, 525-539.

Hals KMD., Berre, I., 2013. Thermal fracturing of geothermal wells and the effects of borehole orientation, *Thirty-Eighth Workshop on Geothermal Reservoir Engineering Stanford University, Stanford, California*, February 11-13, 2013.

Izadi G., Elsworth, D., 2015. The influence of thermal-hydraulic-mechanical- and chemical effects on the evolution of permeability, seismicity and heat production in geothermal reservoirs, *Geothermics* 53, 385–395.

Khalili, N., Selvadurai, APS., 2003. A fully coupled constitutive model for thermo-hydro-mechanical analysis in elastic media with double porosity, *Geophys. Res. Lett*., 30(24), 2268, doi:10.1029/2003GL018838.

Nejati, M., Paluszny, A., Zimmerman, R.W., 2015. A disk-shaped domain integral method for the computation of stress intensity factors using tetrahedral meshes, *International Journal of Solids and Structures*, 69-70, 230-251.

Ogata, A., Banks, R. B., 1961. A solution of the differential equation of longitudinal dispersion in porous media. Technical report, U.S. *Geological Survey*, Washington, D.C.

Paluszny A., Zimmerman R.W. 2011. Numerical simulation of multiple 3D fracture propagation using arbitrary meshes. *Computer Methods in Applied Mechanics and Engineering*, 200, 953-966.

Paluszny A., Zimmerman R.W., 2013. Numerical fracture growth modeling using smooth surface geometric deformation, *Engineering Fracture Mechanics*, 108, 19–36.

Pogacnik, J., Elsworth, D., O'Sullivan, M., O'Sullivan, J., 2016. A damage mechanics approach to the simulation of hydraulic fracturing/shearing around a geothermal injection well, *Computers and Geotechnics* 71, 338–351.

Salimzadeh S., Khalili, N., 2015a. A three-phase XFEM model for hydraulic fracturing with cohesive crack propagation, *Computers and Geotechnics*, 69, 82-92.

Salimzadeh S., Khalili, N., 2015b. A fully coupled XFEM model for flow and deformation in fractured porous media with explicit fracture flow, *International Journal of Geomechanics* (DOI: 10.1061/(ASCE)GM.1943-5622.0000623).

Savitski, A., Detournay, E., 2002. Propagation of a penny-shaped fluid-driven fracture in an impermeable rock: asymptotic solutions, International Journal of *Solids and Structures*, 39 (26), 6311–6337.

Shao, Q., Bouhala1, L., Fiorelli, D., Fahs, M., Younes, A. Núñez, P., Belouettar, S., Makradi, A., 2015, Influence of fluid flow and heat transfer on crack propagation in SOFC multi-layered like material with anisotropic porous layers, *International Journal of Solids and Structures*, DOI: 10.1016/j.ijsolstr.2015.08.026.

Spence DA., Sharp P., 1985. Self-similar solutions for elastohydrodynamic cavity flow, *Proceedings of the Royal Society of London A*, 400:289-313.

Tong, F., Jing, L., Zimmerman, R. W., 2010. A fully coupled thermo-hydro-mechanical model for

simulating multiphase flow, deformation and heat transfer in buffer material and rock masses, *International Journal of Rock Mechanics & Mining Sciences*, 47, 205-217.

Tran, D., Settari, A., Nghiem, L., 2013. Predicting growth and decay of hydraulic-fracture width in porous media subjected to isothermal and nonisothermal flow, *SPE Journal*, SPE 162651.

Wang, Y., Papamichos, E., 1999. Thermal effects on fluid flow and hydraulic fracturing from wellbores and cavities in low-permeability formations, *International Journal for Numerical and Analytical Methods in Geomechanics*, 23, 1819-1834.

Witherspoon, P.A., Wang, J.S.Y., Iwai, K., Gale, J.E., 1980. Validity of cubic law for fluid flow in a deformable rock fracture. *Water Resources Research*, 16, 1016–1024.

Yau, J.F., Wang, S.S., Corten, H.T., 1980. A mixed-mode crack analysis of isotropic solids using conservation laws of elasticity. *ASME Journal of Applied Mechanics*, 47, 335-341.Author, A., Author, B., Author, C. and Author, D.: Example of a journal publication, *Journal*, **xx,** city, (year), 153-166.